Supplementary Information

Gating time constants are the conserved coordinates of cardiac ion channels: a unified reanalysis of seven voltage-clamp corpora

Huan Li

This document contains the identifiability analysis of the thirteen-parameter hERG formulation (S1), the per-corpus extraction methods (S2), the robustness calibres of the conservation verdict (S3), the five-laboratory CiPA dataset methods with its official-table defects and defect registry (S4), the reasons Kir and K2P channels do not enter the verdict (S5), the per-group verdict table (S6), the host-model integration and CiPA scoring details (S7) and the data and code deposition (S8). Every number in the main text resolves to a table here or to the deposited master table.

Contents

S1 Identifiability of the thirteen-parameter hERG formulation **2**

S2 Per-corpus extraction methods **3**

S2.1 Channelpedia . . . 3
S2.2 CiPA five-laboratory hERG . . . 3
S2.3 Lei five-temperature hERG series . . . 3
S2.4 Beattie nine-cell manual hERG dataset . . . 4
S2.5 $Na_v1.5$ two-temperature series . . . 4
S2.6 $Ca_v1.2$ pharmacology dataset . . . 4
S2.7 I_{Ks} activation series . . . 4
S2.8 Reference layers . . . 4

S3 Robustness of the conservation verdict **4**

S4 CiPA five-laboratory dataset: results, official-table defects and registry **6**

S4.1 Central results on the new extraction . . . 6
S4.2 Earlier frozen audit stages carried forward . . . 6
S4.3 Official-table defects found and worked around . . . 6
S4.4 Defect registry . . . 6

S5 Why Kir and K2P do not enter the verdict **7**

S6 Per-group verdict table **8**

S7 Host-model integration and CiPA scoring **12**

S8 Data and code **13**

S1 Identifiability of the thirteen-parameter hERG formulation

The thirteen-parameter hERG scheme is a four-state Markov ring with a double-exponential activation edge, a parallel slow component and a per-cell conductance. It was calibrated on the four protocol families of the construction cell (steady activation, deactivation staircase, sinusoidal wave, action-potential clamp) and passes seven of eight pre-set criteria. The Fisher matrix of Eq. (1) of the main text was assembled by central finite differences (10^{-3} dex steps for log-scaled parameters, $10^{-3}|pf_2|$ for the one linear parameter) on an independent expm simulation channel, weighted by per-segment residual variance. Automatic differentiation was not used; the finite-difference construction is the one whose results are reported.

Table S1: Fisher eigenvalues in ascending order ($\lambda_{\max} = 2.29228 \times 10^9$; condition number 7.3798×10^{12}; span 12.87 orders of magnitude).

index	eigenvalue
1	3.10618×10^{-4}
2	3.14380×10^{4}
3	1.59570×10^{5}
4	4.10533×10^{5}
5	9.83394×10^{5}
6	1.37507×10^{6}
7	2.40444×10^{6}
8	3.30837×10^{6}
9	8.69487×10^{6}
10	5.70476×10^{7}
11	1.57368×10^{8}
12	2.68717×10^{8}
13	2.29228×10^{9}

Null directions are defined as eigenvalues below 10^{-3} of the largest (2.29228×10^6). The count of six is a convention: the sixth eigenvalue sits at 6.0×10^{-4} of the largest and the seventh at 1.05×10^{-3}, on either side of the cut.

Table S2: Null directions below $10^{-3}\lambda_{\max} = 2.29228 \times 10^6$.

#	λ	dominant parameters	interpretation
0	3.1×10^{-4}	$\log_{10} P_1$, $\log_{10} P_{f1}$, $\log_{10} P_2$	activation double-exponential amplitude–component compensation (near-exact null)
1	3.1×10^{4}	$\log_{10} P_2$, $\log_{10} P_{f2}$	voltage-dependence coefficients of the two exponentials compensate
2	1.6×10^{5}	$\log_{10} \alpha_\tau$, $\log_{10} \alpha_{\mathrm{amp}}$, $\log_{10} P_3$	slow-component time constant and amplitude compensate
3	4.1×10^{5}	$\log_{10} P_7$, $\log_{10} P_5$, $\log_{10} P_6$	inactivation–recovery edges compensate
4	9.8×10^{5}	$\log_{10} \alpha_{\mathrm{amp}}$, $\log_{10} P_3$, $\log_{10} \alpha_\tau$	slow amplitude and k_{34} share the rebound peak
5	1.4×10^{6}	$\log_{10} P_3$, $\log_{10} \alpha_{\mathrm{amp}}$, $\log_{10} G_{\mathrm{Kr}}$	absolute-scale triad

One degeneracy is exact rather than numerical. With the maximum open probability frozen, the combination $\alpha_{\mathrm{amp}} \cdot \mathrm{ALPHA} \cdot \mathrm{XMAX}$ enters the likelihood only as a product, so no experiment can separate its factors. A second degeneracy is near-exact: exchanging the two exponential components of the activation edge costs $\lambda/\lambda_{\max} \approx 1.4 \times 10^{-13}$.

The joint rate–conductance rescaling usually assumed in this literature is not a degeneracy of the fitted model. Rescaling all rates by s and the conductance by $1/s$ maps $I(V,t)$ to $s^{-1}I(V,st)$, which

differs from $I(V,t)$ on any fixed protocol time grid. Table S3 quantifies the break: the data already reject a 1% rescaling, and a 10% rescaling moves the predicted waveform by 18–45% depending on protocol.

Table S3: Rate–conductance joint rescaling: relative waveform change Δ_s for the four protocol families. The pre-set criterion was $\Delta < 0.01$ (approximately degenerate) and $\Delta > 0.05$ (broken) at $s = 1.1$; the data break the rescaling already at $s = 1.01$.

protocol	$s = 1.01$	$s = 1.05$	$s = 1.1$	$s = 1.5$	$s = 2.0$
steady activation	0.0233	0.1049	0.1826	0.3796	0.7555
deactivation	0.0258	0.1235	0.2334	0.7587	0.9498
sine wave	0.0553	0.2537	0.4517	0.9614	1.2308
action potential	0.0338	0.1559	0.2831	0.7486	1.0901

The serial-state variant, in which extra closed states are added to repair the peak–sine exclusion, passes all eight criteria but is not identifiable: the Cramér–Rao bounds on its rate multipliers are ±9.6–13.2 dex against a data-supported window of ±0.017 dex, a factor of about 760.

S2 Per-corpus extraction methods

All corpora share one schema and one interval construction (per-row 95% profile likelihood, nuisance parameters refit on a grid over the target, F-statistic threshold). What differs per corpus is the segmentation, the fit windows and the quality-control chain, summarised here.

S2.1 Channelpedia

Automated patch-clamp NWB files with per-cell JSON metadata; 19,282 cells downloaded, 17,987 retained after quality control. Activation, deactivation, inactivation and recovery segments were fit per sweep with mono- or bi-exponential decays (component count fixed per channel family), steady-state curves by Boltzmann fits. Recordings at 15, 25 and 35 °C were used. Groups with fewer than 15 cells do not enter a verdict. Rows whose fit reaches a window or bound are flagged `tau_edge` and retained. Kv1.5 at 15 °C and the K2P rows carry this flag most often.

S2.2 CiPA five-laboratory hERG

Manual patch-clamp per-cell waveforms (62 GB, 14,973 csv files, sha256-verified) of 28 drugs under the standardised ICH S7B Q&A 2.1 protocol with blinded replicate arms. Sweep metadata exist for only two directory trees, so vehicle, drug-block and steady-state windows were segmented from the waveform plateaus alone and the segmentation was then validated against the two metadata-carrying directories. Tail deactivation time constants were extracted per sweep with profile intervals. The per-cell ratio references the steady-state (highest-concentration) window to the vehicle window of the same cell. Of 1,875 cells passing trace-level quality control, 1,750 contribute deactivation windows to the master table and 970 have both segments valid for the ratio. Current-unit suffixes differ across laboratories and were read from the column names (laboratory 2 records amperes, the others pA; the conversion map is part of the frozen pipeline). Voltage-contaminated current columns in three laboratories were detected by a corrupted-column screen and excluded. Defects are registered in S4.

S2.3 Lei five-temperature hERG series

Automated recordings of hERG at 25, 27, 31, 35 and 37 °C (670 wells). Recovery, fast activation and fast deactivation time constants were extracted per well with profile intervals. The 27 °C recovery

batch carries batch noise (a slow tail around 3.2 s), so the temperature law of the main text is stated on the recovery component, which is monotone across the five temperatures.

S2.4 Beattie nine-cell manual hERG dataset

Nine cells, six protocols, manual patch at 37 °C. Steady-state activation was measured by the tail-current method rather than the holding-segment mean; the tail method removes a Boltzmann degeneracy that otherwise pushes midpoint fits to their bounds. Deactivation was fit with two exponential components per sweep.

S2.5 $Na_v1.5$ two-temperature series

Whole-cell Nav1.5 recordings at 25 and 35 °C under five compound levels (four cells). Inactivation time constants were measured from peak-aligned decay windows at 40 µs sampling. Rows reaching the 9 ms fit ceiling at 25 °C are flagged `tau_edge`.

S2.6 $Ca_v1.2$ pharmacology dataset

Six cells with Ca^{2+} and Ba^{2+} charge carriers and a continuous bath-temperature channel recorded alongside every sweep; temperature therefore enters as a measured covariate, not a nominal label. Calcium-dependent inactivation time constants were extracted per sweep. Inactivation under Ba^{2+} is too slow for the 180 ms window; those rows carry the `tau_edge` flag and are excluded from time-constant statistics but retained in the table.

S2.7 I_{Ks} activation series

283 recordings of KCNQ1/KCNE1. Activation delay and time constant were fit jointly on the step epoch; deactivation time constants come from the −40 mV tail epoch. Duplicate recordings of the same cell were resolved to the single best-quality version before fitting.

S2.8 Reference layers

Three reference layers are stored in the master-table schema: official CiPA potency anchors (IC_{50} and Hill coefficients, 29 drugs across seven channels, 250 rows), cross-species group comparisons (38 pairs, 76 rows), and ten gating-layer summaries of 933 deduplicated published models from ICGenealogy whose gating curves were refit in-house (30 rows).

S3 Robustness of the conservation verdict

The headline calibre (D) estimates the group-level true scatter by hierarchical partial pooling with marginal likelihood, propagating per-row profile-likelihood uncertainties (asymmetric half-widths averaged). Three other calibres bracket it: (A) the raw across-cell scatter ratio with no shrinkage; (B) calibre A after removing Boltzmann midpoint fits that hit their voltage bounds; (C) two-stage hierarchical shrinkage with symmetric standard errors. Table S4 gives the Kv-activation verdict under all four.

Across all 194 evaluable groups of the five verdict tables, moving from calibre C to calibre D changes exactly one verdict: Kv1.7 recovery at 15 °C moves from 1.009 to 0.995, sitting on the threshold in both calibres. The hierarchical time-constant estimates differ from the unshrunk values by a median of −1.3% per group, so the scatter estimates are nearly unbiased. The 66-group frame of

Table S4: The Kv-activation verdict under four calibres (64 groups). Calibres differ only in how scatter and uncertainty are estimated; the verdict is unchanged.

calibre	pass	median ratio
A: raw observed scatter	63/64	3.37
B: bound-hit midpoints removed	63/64	2.87
C: hierarchical shrinkage, symmetric errors	63/64	2.48
D: C with profile-likelihood intervals (headline)	63/64	2.48

earlier drafts contained two TASK-3 groups; K2P leak channels have no sigmoidal gating and their inclusion was registered as a grouping impurity, giving the 64-group activation frame used here.

S4 CiPA five-laboratory dataset: results, official-table defects and registry

S4.1 Central results on the new extraction

The drug-versus-vehicle deactivation τ ratio, referenced within cell to the steady-state highest-concentration block window, has pooled median 0.948 ($n = 970$ cells; 43.3% of cells inside the 0.80–1.25 band, 55.4% within ±30%). Per-laboratory medians are 1.05, 0.99, 0.81, 0.92 and 1.17 (laboratories 1–5). The laboratory-3 value, a 19% acceleration, is the largest deviation in the dataset. Stratum medians by steady-state block fraction run 0.96, 0.90, 0.89, 1.01 and 1.07 from shallow to deep block: the ratio does not drift with occupancy. The blinded arm reproduces the unblinded one through the same frozen pipeline (medians 0.87 on $n = 102$ blinded cells against 0.96 on $n = 868$ unblinded). Our per-drug IC_{50} estimates match the official CiPA values within ten-fold for 23 of 24 drugs.

S4.2 Earlier frozen audit stages carried forward

The following dataset-level findings of the frozen audit are independent of the extraction-calibre change and are carried forward unchanged. Cross-laboratory IC_{50} fold differences have median 6.17 over 28 drugs, consistent with the source study's reported natural variability of roughly five-fold. Laboratory 2 is systematically high by 3.10-fold and the shift localises to the addition method: it disappears (0.77) when that laboratory assays real experimental samples. A leak-current explanation was excluded: within-laboratory correlation between holding leak and block is null (laboratory 2, Spearman $\rho = +0.006$, $n = 441$) and the block fraction is computed on a peak-minus-baseline difference, which cancels any constant leak residual. State-dependent binding is visible in three independent waveform signatures: Hill coefficients differ from one in 42 of 134 drug-laboratory sets; the peak-to-plateau shape ratio under deep block is 0.73 in laboratory 1; and 36–39% of first/second exposure segments end before block plateaus. The apparent on-rate of block is flattened by solution exchange (log-log slope against concentration ≈ 0, paired rate ratio 0.32 against a concentration ratio of 10 across 651 pairs), so the dataset pins equilibrium quantities and not binding kinetics. The E-4031 positive-control residual has median 2.4% (IQR 1.5–3.9%) across 1,588 segments, confirming hERG identity of the measured current. Paired two-concentration cells are monotone in block in 643 of 651 pairs (98.8%). The control-segment τ is uncorrelated with series resistance within laboratories (laboratory 1: $\rho = -0.020$, $p = 0.72$, $n = 321$; laboratory 5: $\rho = +0.097$, $p = 0.16$, $n = 208$).

S4.3 Official-table defects found and worked around

Two numerical disasters in the official summary table were found and are registered: the official Hill coefficient for laboratory-5 verapamil reads 299.86 (our refit: 0.81) and for laboratory-5 risperidone 101.55 (our refit: 0.64). Official table-level values were therefore used only after independent refit. Concentration units coexist in three notations across directories and were normalised per directory. Current-unit suffixes differ across laboratories (laboratory 2 records amperes); a first leak-audit pass that read columns by position without the unit map produced an artefactual all-zero leak report, was caught by manual cross-checking, and was rerun with the unit map (laboratory 1 median holding leak −28.6 pA). Intended protocol templates cannot substitute for the measured voltage column: template-based reconstruction returns control time constants 12.96-fold too slow (laboratory 1) and 0.14-fold too fast (laboratory 2).

S4.4 Defect registry

Registered defects, distilled from the method archive (22 entries on record): laboratories 1 and 2 files lack temperature and voltage columns; laboratory 5 vehicle rundown is 9.1% (four times

the other laboratories) with per-file voltage drift; laboratory 2 signal amplitude is one order of magnitude lower (84 pA versus 1.2–2.0 nA); laboratory 4 E-4031 reference residual is high (12.2%) and its series-resistance records are a constant nominal 80 MΩ (82 cells, not measured, excluded from correlation analysis); laboratory 3 carries no CellProperties metadata, consistent with the published reviewer response that laboratory 3 applied no series-resistance compensation; exposure generally does not plateau, so IC_{50} values are biased upward; current-unit suffixes differ across laboratories. None of these defects touches the τ-conservation conclusion, for which laboratory 3 is the least-affected gold-standard arm.

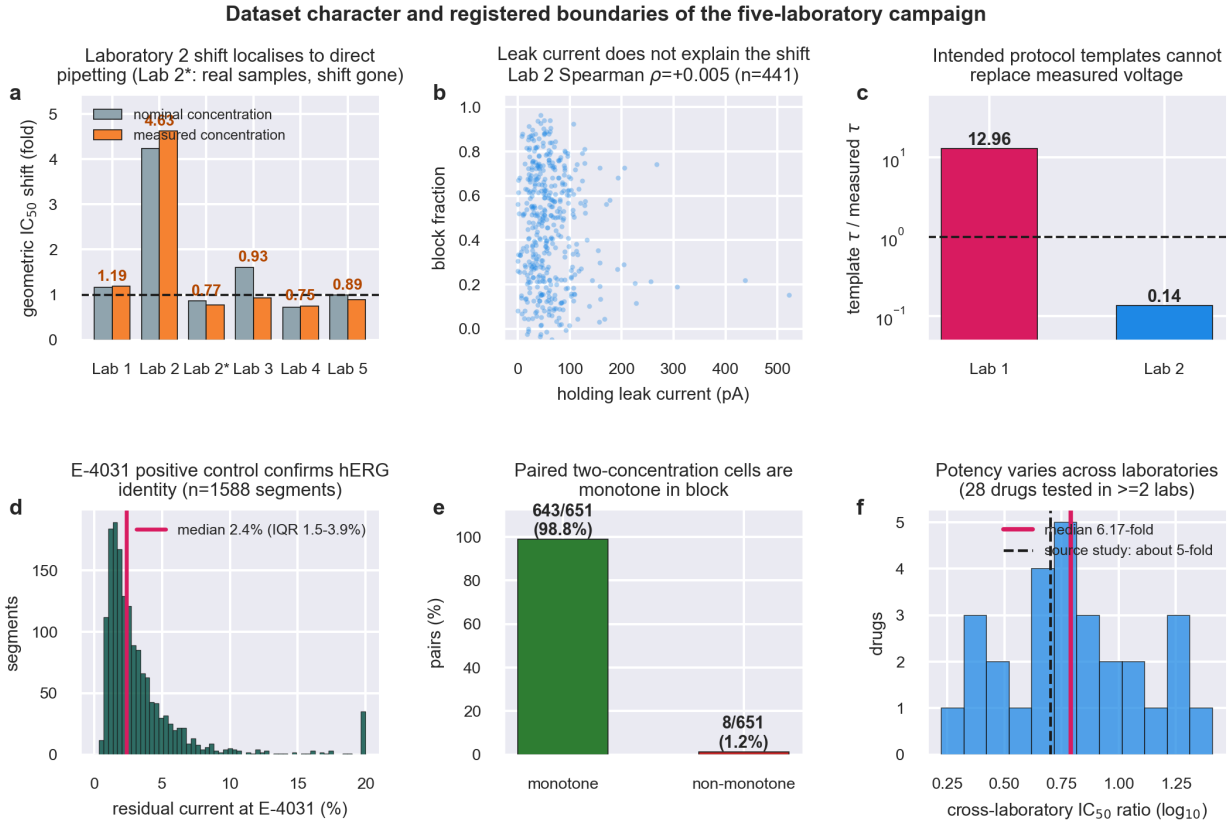


Figure S1: **Dataset character and registered boundaries of the five-laboratory campaign.** (a) Per-laboratory geometric IC_{50} shift with nominal and measured concentrations; laboratory 2 assayed on real samples (laboratory 2*) loses its shift (0.77). (b) Holding leak current versus block fraction in laboratory 2 (Spearman $\rho = +0.006$, $n = 441$). (c) Template-voltage reconstruction returns control time constants 12.96-fold too slow (laboratory 1) and 0.14-fold too fast (laboratory 2), so intended-protocol templates cannot replace measured voltage. (d) E-4031 positive-control residuals (median 2.4%, IQR 1.5–3.9%, $n = 1{,}588$ segments). (e) Paired two-concentration cells are monotone in block in 643 of 651 pairs (98.8%). (f) Cross-laboratory IC_{50} ratios (median 6.17-fold, $n = 28$ drugs; source-study expectation about five-fold).

S5 Why Kir and K2P do not enter the verdict

The verdict rule requires two scatters per group: a time constant and a Boltzmann midpoint. Kir channels carry inward-rectifier currents whose quasi-steady-state curves are rectification-dominated rather than S-shaped, so no Boltzmann midpoint exists to scatter; a large fraction of Kir cells is silent at the holding potential used by the recording protocol, which removes the tail segments needed for deactivation fits. K2P channels are leak channels: their currents are instantaneously open rectifiers without gated S-shaped curves, and the two TASK-3 groups that had been carried

in an earlier 66-group frame were removed as a grouping impurity. Both families remain in the master table with their extracted quantities and flags; they simply have no well-posed midpoint axis on which the verdict could run. Pure leak currents are subtracted in every corpus by the same peak-minus-baseline construction.

S6 Per-group verdict table

Table S5: Per-group conservation verdicts. Ratio (obs) is the raw scatter ratio; Ratio (shrunk) is the headline calibre (hierarchical partial pooling with profile-likelihood per-row uncertainties); Pass marks shrunk ratio above one. Groups with too few valid midpoint fits for shrinkage are marked n/a and do not enter the pass counts. [a]Raw ratio off scale: bound-hit Boltzmann fits collapse the slope normalisation; calibre B removes exactly such fits.

Layer	Channel	Temp (°C)	Ratio (obs)	Ratio (shrunk)	Pass
HCN activation	HCN1	15	8.25	8.03	yes
HCN activation	HCN1	25	11.79	9.96	yes
HCN activation	HCN2	25	14.29	13.49	yes
HCN activation	HCN4	25	3.43	3.70	yes
HCN activation	HCN4	35	5.07	5.31	yes
Kv activation	Kv1.1	15	9.39	3.09	yes
Kv activation	Kv1.1	25	10.50	5.22	yes
Kv activation	Kv1.1	35	4.39	4.43	yes
Kv activation	Kv1.2	15	1.60	1.58	yes
Kv activation	Kv1.2	25	1.90	1.86	yes
Kv activation	Kv1.2	35	3.88	3.79	yes
Kv activation	Kv1.3	15	22.61	4.51	yes
Kv activation	Kv1.3	25	3.48	3.38	yes
Kv activation	Kv1.3	35	3.59	3.52	yes
Kv activation	Kv1.4	15	10.93	2.52	yes
Kv activation	Kv1.4	25	3.43	3.27	yes
Kv activation	Kv1.4	35	3.03	3.19	yes
Kv activation	Kv1.5	15	2.89	1.33	yes
Kv activation	Kv1.5	25	2.16	1.97	yes
Kv activation	Kv1.5	35	11.71	2.85	yes
Kv activation	Kv1.6	15	3.32	3.24	yes
Kv activation	Kv1.6	25	2.97	2.92	yes
Kv activation	Kv1.6	35	17.57	5.08	yes
Kv activation	Kv1.7	15	15.85	2.31	yes
Kv activation	Kv1.7	25	1.98	1.89	yes
Kv activation	Kv1.7	35	3.55	2.87	yes
Kv activation	Kv10.1	15	1.91	1.90	yes
Kv activation	Kv10.1	25	3.95	3.48	yes
Kv activation	Kv10.1	35	3.09	3.05	yes
Kv activation	Kv10.1_003	15	1.30	1.28	yes
Kv activation	Kv10.1_003	25	3.71	1.14	yes
Kv activation	Kv10.1_003	35	4.37	3.07	yes

continued on next page

Table S5 (continued)

Layer	Channel	Temp (°C)	Ratio (obs)	Ratio (shrunk)	Pass
Kv activation	Kv10.2	35	10.57	4.13	yes
Kv activation	Kv12.1	15	9.31	2.83	yes
Kv activation	Kv12.1	25	3.57	2.94	yes
Kv activation	Kv12.1	35	8.19	1.87	yes
Kv activation	Kv12.3	15	8.46	6.33	yes
Kv activation	Kv12.3	25	12.36	7.22	yes
Kv activation	Kv12.3	35	15.25	8.02	yes
Kv activation	Kv2.1	15	2.53	2.49	yes
Kv activation	Kv2.1	25	2.78	2.66	yes
Kv activation	Kv2.1	35	2.52	2.46	yes
Kv activation	Kv2.1_C1	25	2.61	2.43	yes
Kv activation	Kv2.2	15	1.97	1.87	yes
Kv activation	Kv2.2	25	2.98	1.79	yes
Kv activation	Kv2.2	35	2.96	2.93	yes
Kv activation	Kv3.1	15	1.65	1.32	yes
Kv activation	Kv3.1	25	1.21	1.17	yes
Kv activation	Kv3.1	35	1.38	1.67	yes
Kv activation	Kv3.2	15	0.82	0.43	no
Kv activation	Kv3.2	25	1.13	1.07	yes
Kv activation	Kv3.2	35	1.82	1.64	yes
Kv activation	Kv3.3	15	1.84	1.69	yes
Kv activation	Kv3.3	25	1.58	1.57	yes
Kv activation	Kv3.3	35	2.02	2.27	yes
Kv activation	Kv3.4	15	1.85	1.82	yes
Kv activation	Kv3.4	25	4.05	2.05	yes
Kv activation	Kv3.4	35	3.14	1.50	yes
Kv activation	Kv4.1	15	12.48	2.00	yes
Kv activation	Kv4.1	25	9.24	3.56	yes
Kv activation	Kv4.1	35	3.95	3.68	yes
Kv activation	Kv4.2	15	11.10	2.48	yes
Kv activation	Kv4.2	25	6.86	1.11	yes
Kv activation	Kv4.2	35	5.91	1.79	yes
Kv activation	Kv4.3	15	3.09	1.97	yes
Kv activation	Kv4.3	25	2.37	2.31	yes
Kv activation	Kv4.3	35	2.82	2.04	yes
Kv activation	Kv7.1	15	4.62	3.63	yes
Kv activation	Kv7.2D1	15	9.70	3.69	yes
Kv recovery	Kv1.1	15	4.20	3.59	yes
Kv recovery	Kv1.1	25	6.14	4.65	yes
Kv recovery	Kv1.1	35	4.25	3.95	yes
Kv recovery	Kv1.2	15	2.57	2.73	yes
Kv recovery	Kv1.2	25	4.13	3.78	yes
Kv recovery	Kv1.2	35	3.32	6.12	yes
Kv recovery	Kv1.3	15	5.44	4.59	yes
Kv recovery	Kv1.3	25	2.27	2.35	yes
Kv recovery	Kv1.3	35	1.85	2.15	yes
Kv recovery	Kv1.4	15	2.33	2.01	yes
Kv recovery	Kv1.4	25	1.56	1.28	yes
Kv recovery	Kv1.4	35	2.37	1.84	yes

continued on next page

Table S5 (continued)

Layer	Channel	Temp (°C)	Ratio (obs)	Ratio (shrunk)	Pass
Kv recovery	Kv1.5	15	1.21	1.24	yes
Kv recovery	Kv1.5	25	3.06	2.68	yes
Kv recovery	Kv1.5	35	2.66	2.09	yes
Kv recovery	Kv1.6	15	6.35	4.17	yes
Kv recovery	Kv1.6	25	6.40	5.06	yes
Kv recovery	Kv1.6	35	5.16	4.62	yes
Kv recovery	Kv1.7	15	1.34	1.00	no
Kv recovery	Kv1.7	25	1.32	1.26	yes
Kv recovery	Kv10.1	25	1.40	1.16	yes
Kv recovery	Kv2.1	15	2.52	2.37	yes
Kv recovery	Kv2.1	25	3.00	2.88	yes
Kv recovery	Kv2.1	35	2.74	2.72	yes
Kv recovery	Kv2.1_C1	25	2.31	2.97	yes
Kv recovery	Kv2.2	15	3.48	1.20	yes
Kv recovery	Kv2.2	25	5.96	3.04	yes
Kv recovery	Kv2.2	35	1.57	1.77	yes
Kv recovery	Kv3.1	15	0.98	0.91	no
Kv recovery	Kv3.1	25	1.97	1.99	yes
Kv recovery	Kv3.1	35	2.41	2.43	yes
Kv recovery	Kv3.2	15	2.19	1.86	yes
Kv recovery	Kv3.2	25	1.28	1.26	yes
Kv recovery	Kv3.3	15	1.98	2.50	yes
Kv recovery	Kv3.3	25	1.92	2.14	yes
Kv recovery	Kv3.3	35	2.44	2.14	yes
Kv recovery	Kv3.4	15	0.80	0.86	no
Kv recovery	Kv3.4	25	1.35	1.43	yes
Kv recovery	Kv4.1	15	1.20	1.22	yes
Kv recovery	Kv4.1	25	1.49	2.35	yes
Kv recovery	Kv4.3	15	1.36	1.05	yes
Kv recovery	Kv4.3	25	1.23	1.40	yes
Kv deactivation	Kv1.1	15	6.99	3.77	yes
Kv deactivation	Kv1.1	25	6.62	3.32	yes
Kv deactivation	Kv1.1	35	3.96	3.10	yes
Kv deactivation	Kv1.2	15	3.35	3.35	yes
Kv deactivation	Kv1.2	25	2.85	2.86	yes
Kv deactivation	Kv1.2	35	3.83	2.95	yes
Kv deactivation	Kv1.3	15	13.75	4.50	yes
Kv deactivation	Kv1.3	25	2.99	2.93	yes
Kv deactivation	Kv1.3	35	3.07	3.06	yes
Kv deactivation	Kv1.4	15	2.67	0.61	no
Kv deactivation	Kv1.4	25	0.97	0.83	no
Kv deactivation	Kv1.5	15	4.63	2.14	yes
Kv deactivation	Kv1.5	25	1.93	2.10	yes
Kv deactivation	Kv1.5	35	10.64	2.59	yes
Kv deactivation	Kv1.6	15	2.30	2.66	yes
Kv deactivation	Kv1.6	25	2.77	2.85	yes
Kv deactivation	Kv1.6	35	12.53	3.28	yes
Kv deactivation	Kv1.7	15	3.39	n/a	n/a
Kv deactivation	Kv1.7	25	1.02	n/a	n/a

continued on next page

Table S5 (continued)

Layer	Channel	Temp (°C)	Ratio (obs)	Ratio (shrunk)	Pass
Kv deactivation	Kv10.1	15	5.11	6.18	yes
Kv deactivation	Kv10.1	25	5.09	4.55	yes
Kv deactivation	Kv10.1	35	1.24	n/a	n/a
Kv deactivation	Kv10.1_003	15	1.31	1.33	yes
Kv deactivation	Kv10.1_003	25	16.69	5.34	yes
Kv deactivation	Kv10.1_003	35	3.26	n/a	n/a
Kv deactivation	Kv12.1	15	5.64	4.93	yes
Kv deactivation	Kv12.1	25	2.94	2.49	yes
Kv deactivation	Kv12.1	35	15.57	4.80	yes
Kv deactivation	Kv12.3	25	12.05	9.66	yes
Kv deactivation	Kv12.3	35	11.67	n/a	n/a
Kv deactivation	Kv2.1	15	2.50	2.60	yes
Kv deactivation	Kv2.1	25	2.90	2.80	yes
Kv deactivation	Kv2.1	35	2.02	2.46	yes
Kv deactivation	Kv2.1_C1	25	3.36	3.14	yes
Kv deactivation	Kv2.2	15	1.82	1.68	yes
Kv deactivation	Kv2.2	25	2.50	1.56	yes
Kv deactivation	Kv2.2	35	3.75	4.19	yes
Kv deactivation	Kv3.1	15	2.74	2.34	yes
Kv deactivation	Kv3.1	25	3.55	3.81	yes
Kv deactivation	Kv3.1	35	1.65	1.94	yes
Kv deactivation	Kv3.2	15	2.44	1.33	yes
Kv deactivation	Kv3.2	25	3.56	3.42	yes
Kv deactivation	Kv3.2	35	4.27	4.45	yes
Kv deactivation	Kv3.3	15	3.49	3.33	yes
Kv deactivation	Kv3.3	25	3.23	3.41	yes
Kv deactivation	Kv3.3	35	0.92	0.88	no
Kv deactivation	Kv3.4	15	1.30	1.15	yes
Kv deactivation	Kv3.4	25	4.47	2.33	yes
Kv deactivation	Kv3.4	35	3.38	2.25	yes
Kv deactivation	Kv4.1	15	5.41	0.89	no
Kv deactivation	Kv4.1	25	3.67	n/a	n/a
Kv deactivation	Kv4.3	15	1.63	1.05	yes
Kv deactivation	Kv4.3	25	0.69	n/a	n/a
Kv deactivation	Kv7.1	15	0.56	0.56	no
Kv deactivation	Kv7.2D1	15	2.93	1.94	yes
Kv inactivation	Kv1.1	15	10.04	n/a	n/a
Kv inactivation	Kv1.1	25	5.96	2.97	yes
Kv inactivation	Kv1.1	35	3.38	3.24	yes
Kv inactivation	Kv1.2	25	2.05	1.98	yes
Kv inactivation	Kv1.2	35	2.27	2.22	yes
Kv inactivation	Kv1.3	15	11.83	2.42	yes
Kv inactivation	Kv1.3	25	1.36	1.33	yes
Kv inactivation	Kv1.3	35	1.21	1.18	yes
Kv inactivation	Kv1.4	15	8.66	1.89	yes
Kv inactivation	Kv1.4	25	2.40	2.18	yes
Kv inactivation	Kv1.4	35	2.78	2.89	yes
Kv inactivation	Kv1.5	15	2.19	n/a	n/a
Kv inactivation	Kv1.5	25	1.15	1.05	yes

continued on next page

Table S5 (continued)

Layer	Channel	Temp (°C)	Ratio (obs)	Ratio (shrunk)	Pass
Kv inactivation	Kv1.5	35	5.08	1.24	yes
Kv inactivation	Kv1.6	15	2.05	n/a	n/a
Kv inactivation	Kv1.6	25	2.48	2.45	yes
Kv inactivation	Kv1.6	35	15.77	4.02	yes
Kv inactivation	Kv1.7	15	8.74	1.07	yes
Kv inactivation	Kv1.7	25	1.53	1.52	yes
Kv inactivation	Kv1.7	35	3.16	3.71	yes
Kv inactivation	Kv10.1_003	25	4.37	n/a	n/a
Kv inactivation	Kv12.1	35	25.05	n/a	n/a
Kv inactivation	Kv2.1	15	off-scale[a]	n/a	n/a
Kv inactivation	Kv2.1	25	1.25	1.19	yes
Kv inactivation	Kv2.1	35	1.33	1.30	yes
Kv inactivation	Kv2.1_C1	25	0.98	0.91	no
Kv inactivation	Kv2.2	15	6.66	n/a	n/a
Kv inactivation	Kv2.2	25	1.07	0.64	no
Kv inactivation	Kv2.2	35	1.45	1.45	yes
Kv inactivation	Kv3.1	25	0.81	n/a	n/a
Kv inactivation	Kv3.1	35	0.96	0.85	no
Kv inactivation	Kv3.2	25	0.77	0.73	no
Kv inactivation	Kv3.2	35	1.07	1.01	yes
Kv inactivation	Kv3.3	15	1.72	1.02	yes
Kv inactivation	Kv3.3	25	0.91	0.90	no
Kv inactivation	Kv3.3	35	1.01	1.00	yes
Kv inactivation	Kv3.4	15	0.50	0.50	no
Kv inactivation	Kv3.4	25	1.86	0.94	no
Kv inactivation	Kv3.4	35	1.10	1.12	yes
Kv inactivation	Kv4.1	15	10.02	1.61	yes
Kv inactivation	Kv4.1	25	7.35	2.96	yes
Kv inactivation	Kv4.2	15	11.96	n/a	n/a
Kv inactivation	Kv4.3	15	2.90	1.85	yes
Kv inactivation	Kv4.3	25	3.20	3.08	yes
Kv inactivation	Kv4.3	35	0.86	n/a	n/a
Kv inactivation	TASK3	35	2.42	n/a	n/a

S7 Host-model integration and CiPA scoring

Table S6 gives the host-level acceptance checks J1–J6 for the O'Hara–Rudy composite with measured-table I_{Kr} and I_{Ks}. Table S7 gives the per-arm CiPA scoring on the 24 shared risk-labelled drugs.

The cross-laboratory carry test of the main text substitutes the Channelpedia population hERG time-constant table for the sealed single-cell kinetics and scores the prediction of CiPA screening traces cell by cell under the frozen acceptance criteria. The population-table model passes 67 of 68 cells (laboratory 3: 20/20; laboratory 4: 16/16; laboratory 5: 29/32; manual: 3/3), against 65 of 68 for the sealed-table model, and no cell moves from pass to fail. The two rescued cells sit in laboratory 5, whose recordings carry the largest voltage-clamp uncertainty of the panel.

Table S6: Host-level checks J1–J6 for the O'Hara–Rudy composite with measured-table I_{Kr} and I_{Ks}.

check	content	measured	band
J1	last-10-beat APD90 range	0.005 ms	< 0.5 ms
J2	APD90 / APA / RMP / qNet	251.206 ms (Δ0.36%) / 128.51 mV / -87.99 mV / 0.056	APD90 $\pm$2%; APA 124.4–130; RMP -95 to -85
J3a	I_{Kr}-only swap, trace agreement	1.1×10^{-5}	$\leq 1\%$
J3b	I_{Ks}-only swap	APD90 255.77; APA 127.94; RMP -88.00; qNet 0.0717	all in band
J3c	N-arm registration	APA saturated; ΔAPA $= 3.1 \times 10^{-5}$ mV at $G \times 16$	expected-failure signature
J4	upstroke dV/dt_{max}	240.7 vs. 236.6 V/s (1.017)	50–500 V/s
J5	rate dependence	monotone shortening; 1:1 capture; max difference 2.5 ms	monotone + capture
J6	peak-current ratios	I_{Kr} 2.06; I_{Ks} 1.52; I_{Na} 0.997; I_{CaL} 0.979; I_{NaL} 1.009; I_{to} 1.002; I_{K1} 1.004	all in 0.2–5

Table S7: CiPA scoring arms on the 24 shared drugs.

arm	model	V1 ρ	V2 AUC
B1	official Markov 9-state + static Hill	-0.523	0.833
B2s	measured-table + static binding	-0.506	0.833
B2	measured-table + dynamic binding	-0.547 ($p = 0.0057$)	0.857

S8 Data and code

All source datasets are public; their repository identifiers are listed in Table 1 of the main text. The unified master table (487,940 rows including the 356 reference-layer rows), the extraction and verdict code, the figure scripts and the per-layer verdict tables are deposited at Zenodo (https://doi.org/10.5281/zenodo.23042211) and mirrored at GitHub (https://github.com/lihuanlz/alpha-ion-channel-models). The earlier four-channel preprint is at Research Square (https://doi.org/10.21203/rs.3.rs-11218939/v1).